elaTCSF: A Temporal Contrast Sensitivity Function for Flicker Detection and Modeling Variable Refresh Rate Flicker

YANCHENG CAI, University of Cambridge, United Kingdom
ALI BOZORGIAN, Norwegian University of Science and Technology, Norway
MALIHA ASHRAF, University of Cambridge, United Kingdom
ROBERT WANAT, LG Electronics North America, United States of America
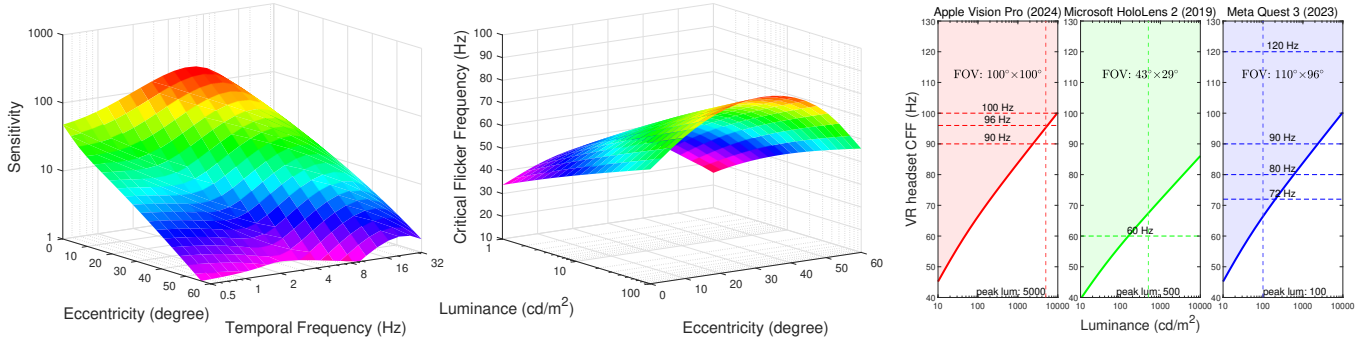RAFAŁ K. MANTIUK, University of Cambridge, United Kingdom

Fig. 1. Left: 3D Visualization of elaTCSF. elaTSCF predicts sensitivity and critical flicker frequency along three dimensions: Eccentricity, Luminance, and Area. Right: elaTCSF predicts flicker visibility in devices with varying field-of-view and luminance, such as VR headsets listed in the plots on the right. The dashed lines indicate the current display capabilities (peak luminance and official refresh rate). Above the CFF threshold (colored area), flicker is unlikely to be visible.

The perception of flicker has been a prominent concern in illumination and electronic display fields for over a century. Traditional approaches often rely on Critical Flicker Frequency (CFF), primarily suited for high-contrast (full-on, full-off) flicker. To tackle varying contrast flicker, the International Committee for Display Metrology (ICDM) introduced a Temporal Contrast Sensitivity Function $TCSF_{IDMS}$ within the Information Display Measurements Standard (IDMS). Nevertheless, this standard overlooks crucial parameters: luminance, eccentricity, and area. Existing models incorporating these parameters are inadequate for flicker detection, especially at low spatial frequencies. To address these limitations, we extend the $TCSF_{IDMS}$ and combine it with a new spatial probability summation model to incorporate the effects of luminance, eccentricity, and area (elaTCSF). We train the elaTCSF on various flicker detection datasets and establish the first variable refresh rate flicker detection dataset for further verification. Additionally, we contribute to resolving a longstanding debate on whether the flicker is more visible in peripheral vision. We demonstrate how elaTCSF can be used to predict flicker due to low-persistence in VR headsets, identify flicker-free VRR operational ranges, and determine flicker sensitivity in lighting design.

CCS Concepts: • **Computing methodologies** → **Perception**;

Additional Key Words and Phrases: flicker detection, variable refresh rate, contrast sensitivity, visual perception

1 INTRODUCTION

Flicker, known as temporal light modulation (TLM), has been a significant concern in illumination engineering for over a century. It has detrimental effects on human physiology, ranging from irritation to neurological disturbances [Miller et al. 2023]. Flicker has been observed in different technologies such as fluorescent lamps [Eastman and Campbell 1952] in the 1940s, cathode-ray tubes (CRTs) [Bauer et al. 1983] in the 1980s, and LED [Lehman et al. 2011].

The Critical Flicker Frequency (CFF) is the best-known flicker detection standard that has been in use for over a century [Porter 1902], defined as the frequency at which a flickering light becomes indistinguishable from a steady, non-flickering light. However, it assumes a high-contrast flicker (light on and off), which is not always applicable. For example, flicker found in variable refresh rate (VRR) displays is caused by slight luminance differences at varying refresh rates, resulting in a low-contrast flicker. To address flicker of various contrast, Watson proposed a flicker detection metric [Watson and Ahumada 2011], which relies on the Temporal Contrast Sensitivity Function (TCSF) equation from [Watson et al. 1986]. This metric

(TCSF$_{IDMS}$[1]) was later incorporated into the information display measurements standard (IDMS) v1.2 by the International Committee Display Metrology (ICDM) and was released in 2023. However, as acknowledged by Watson and Ahumada [2011], other factors such as luminance, area, and eccentricity also affect the shape of TCSF, yet these parameters have not been integrated into the current standard, limiting its applications. Existing Contrast Sensitivity Functions (CSFs), such as Barten's [1999], stelaCSF [Mantiuk et al. 2022] and castleCSF [Ashraf et al. 2024] predict sensitivity as a function of mentioned factors, but (a) do not offer sufficient accuracy at high temporal frequencies for modeling flicker; (b) cannot explain flicker visibility for large sources that span a significant portion of the visual field. This paper aims to extend the TCSF$_{IDMS}$ to incorporate the effects of eccentricity, luminance and area (hence elaTCSF), updating the standard for flicker detection.

A 120-year-long debate persists in flicker detection: Is temporal sensitivity to flicker higher in the peripheral visual field (parafovea) than in the central (fovea)? The organization of the visual field is topographically represented in the striate cortex, with central regions receiving a disproportionately larger representation than peripheral areas [Daniel and Whitteridge 1961]. However, regarding temporal sensitivity, experimental measurements are conflicting and puzzling: some researchers observe a rise and fall in CFF with increasing eccentricity, peaking in the parafovea [Hartmann et al. 1979; Hylkema 1942; Krajancich et al. 2021; Phillips 1933; Porter 1902; Rovamo and Raninen 1984; Tyler 1987], while others contend that temporal sensitivity peaks at fovea and decreases steadily with eccentricity [Chapiro et al. 2023; Ross 1936]. Presently, a consensus remains elusive, although the data from Hartmann et al. [1979] shows that larger stimulus areas, higher luminances, and higher contrasts are more likely to elicit peaks in the parafovea. We rely on those findings, including modern functional magnetic resonance imaging (fMRI) measurements of cortex activity [Himmelberg and Wade 2019; Horiguchi et al. 2009], and propose a model that can explain these seemingly conflicting observations.

Larger signal areas generally activate a broader range of retinal cone and rod cells, enhancing human sensitivity. Some CSF models like castleCSF [Ashraf et al. 2024] have incorporated area (size) as a crucial parameter. However, they treat area and eccentricity as independent parameters. In reality, for stimuli with large areas, a range of eccentricities is involved, particularly evident in our VRR flicker dataset, which includes full-screen flicker. Relying solely on one eccentricity value is evidently insufficient. In this context, we propose a spatial probability summation model that can work with stimuli spanning any portion of the visual field.

In summary, our contributions are as follows:

- We introduce elaTCSF with a spatial probability summation model [2], which accounts for eccentricity, luminance, and area, extending the industry flicker detection standard TCSF$_{IDMS}$. We also address past controversies regarding parafovea sensitivity peak.

- We measure the visibility of flicker on a VRR display. The measurements are combined with publicly available flicker detection data to calibrate and test elaTCSF. The dataset will be made publicly available.
- We demonstrate several applications of the model, including predicting safe refresh rate ranges for VRR displays, addressing VR headsets low-persistence flicker, and assisting in lighting design.

2 RELATED WORK

2.1 Temporal sensitivity and Critical Flicker Frequency

The neurons in the retina, thalamus, and subsequent stages of the visual pathway are sensitive to temporal variations in the retinal image [Breitmeyer and Julesz 1975; Robson 1966; Rucci et al. 2018]. The sensitivity of human observers to temporal variations in light intensity has been extensively measured through psychophysical experiments [de Lange Dzn 1958; Hartmann et al. 1979; Kelly 1961; Kong et al. 2018; Robson 1966; Tyler 1987]. Some researchers [Chapiro et al. 2023; Hartmann et al. 1979; Hecht and Verrijp 1933; Krajancich et al. 2021; Porter 1902] have focused on determining the frequency at which full-depth temporal modulation fuses to a steady light, known as CFF. CFF serves as a behavioral measure of temporal resolution [Donner 2021]. Understanding CFF aids in predicting when the human visual system becomes insensitive to flicker, crucial for lighting systems design [Watson et al. 1986]. The Ferry–Porter law [Porter 1902] explains the variation of CFF as a function of luminance and the Granit–Harper law [Granit and Harper 1930] as the function of stimulus area.

2.2 Flicker visibility metrics

Watson and Ahumada [2015] extended their prior flicker visibility metric [Watson and Ahumada 2011] to account for the effects of luminance. They employed a bilinear TCSF model, fitted to the high-temporal-frequency limbs of the flicker detection measurements reported by [de Lange Dzn 1958]. Additionally, they assume that the Ferry-Porter law applies not only to CFF (contrast equal to one) but also to contrasts lower than one. This metric reports visibility in terms of Just Noticeable Differences (JNDs).

Farrell [1986] proposed a method to predict visible flicker in displays. It relies on the idea that, in a temporal amplitude sensitivity plot with double logarithmic axes, curves for different luminance levels converge to a common high-temporal-frequency asymptote (see [Kelly 1961], for a critical view, see [Rider et al. 2019]), rendering CFF independent of adapting luminance. Note that this trend does not hold for contrast sensitivity curves.

2.3 Variable Refresh Rate Flicker (VRR)

A Graphics Processing Unit (GPU) renders frames at varying rates, which do not align with a display's fixed refresh rate. Traditionally, a GPU used a vertical synchronization signal (VSync) to ensure frames are displayed only when fully drawn. VSync, however, could cause skipped frames (stutter) and introduce unnecessary latency. To allow adaptive frame rate and reduce the latency, NVIDIA introduced VRR technology in 2013. VRR relies on the display holding pixel intensity for varying amounts of time, e.g., with capacitors in LCD panels

---

[1]TCSF describes human visual sensitivity as a function of temporal frequency, exhibiting diverse forms. TCSF$_{IDMS}$ specifically denotes the standard proposed by the International Committee for Display Metrology (https://www.sid.org/Standards/ICDM).
[2]The code for the model and the datasets used to train it can be found on the project page: https://www.cl.cam.ac.uk/research/rainbow/projects/elaTCSF/.
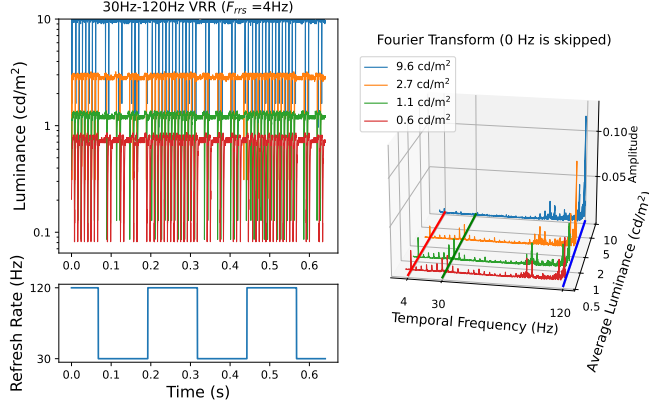
Fig. 2. Left: Measurement of a VRR display, which alternates between 30 Hz and 120 Hz in short time intervals. The upper plot shows drops in luminance (caused by Vertical Blanking Interval (V-blank)) that vary in frequency depending on the refresh rate. The differences in the frequency of those drops cause small luminance differences and result in flicker. Right: The same signal in the frequency domain shows peaks at 4 Hz (the frequency of the refresh rate change), 30 Hz and 120 Hz (caused by V-blanks).
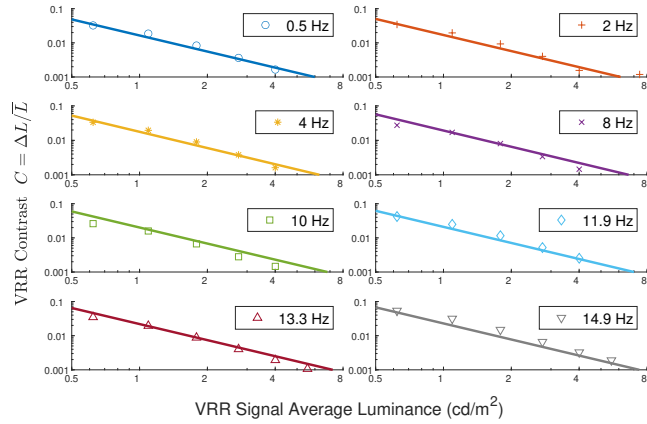

Fig. 3. The contrast of VRR flicker at varying stimulus luminance and temporal frequencies or refresh rate switch, F_{rrs} [Hz]. Luminance levels above 8 cd/m^2 are irrelevant to us because none of our VRR experimental data reaches above that luminance.

[Slavenburg et al. 2020]. In VRR mode, minor differences in display luminance at various refresh rates create low-frequency components in the Fourier domain, leading to visible flicker. Such flicker typically has low contrast and cannot be explained by the CFF models and data. Our aim is to develop a model that can explain VRR flicker.

3 VRR FLICKER SENSITIVITY EXPERIMENT

To model the visibility of flicker found in VRR displays, we conducted measurements on a VRR-capable (G-Sync) OLED display. Based on these measurements, we designed a psychophysical flicker detection experiment to measure human observers' sensitivity to VRR flicker under varying conditions.
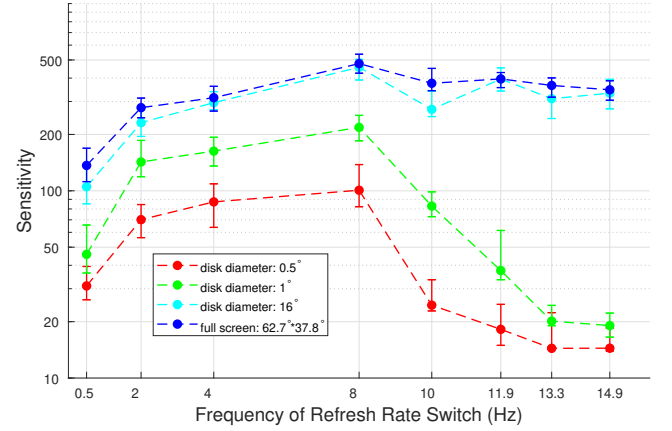

Fig. 4. Our VRR Flicker dataset, where each point represents the average sensitivity across all participants. The error bars indicate the upper and lower bounds derived from psychometric function fitting.

Fig. 5. A photograph of the experimental setup. The experiment was taken in a dark room. The lights were added to take a photo and were not present during the experiment.

Display Equipment. The measurements were conducted on an LG OLED G1 55" 4K Smart TV, chosen because it represents modern VRR displays and exhibits VRR flicker at low luminance levels. Moreover, its size is large enough to support flicker experiments over a very wide field of view. We measured the uniformity of the display and found the luminance difference between the central part and the edges to be less than 10%.

VRR Flicker Stimuli. The stimuli were discs of varying sizes (0.5, 1, and 16 visual degrees in diameter) and a rectangular uniform field occupying the entire screen (62.7° × 37.8°). The discs were shown on a black background. To induce flicker, the refresh rate was switched between 30 and 120 Hz in a square-wave pattern (see Figure 2-bottom-left). The frequency of refresh rate switch (F_{rrs}) varied between 0.5 and 14.9 Hz.

Display calibration and measurements. Since the primary cause of VRR flicker is the subtle luminance differences across varying refresh rates, these differences result in low-frequency components

in the Fourier domain, causing perceptible flicker. Therefore, flicker visibility is linked to the average screen luminance. We measured absolute display luminance levels with the Konica Minolta Chroma Meter CS-200. Temporal variation in luminance was measured with the Topcon Luminance Colorimeter RD-80SA, which provides a fast analog channel response of less than 80 μs. Figure 2-left visualizes some temporal measurement results. The subtle luminance differences between 30 Hz and 120 Hz produce low-frequency components in the Fourier transform frequency domain, as shown in Figure 2-right. We transform the signal into the frequency domain to identify the fundamental frequency (matching F_{rrs}). The flicker contrast is calculated as the ratio of the modulation amplitude at the fundamental frequency to the mean luminance of the VRR stimulus: $C = \Delta L / \bar{L}$.

Based on the above measurements, we can model flicker contrast as the function of display luminance and F_{rrs}, as shown in Figure 3. The flicker contrast did not depend on the size of the displayed pattern in our measurements.

Experimental Procedure. Due to the characteristics of VRR flicker, we cannot directly control its contrast. Instead, we rely on the fact that the contrast of the flicker increases as we lower the luminance of the stimulus (see Figure 3). Therefore, the observers directly adjusted luminance and indirectly contrast in our experiments.

The detection thresholds were measured in two stages. First, the observers were instructed to adjust the luminance of each VRR stimulus until they could just detect flicker (method-of-adjustment). The adjusted luminance was then used as a starting point (a prior) for the 2-interval-forced-choice experiment. In this stage, the observers were presented with two intervals in random order: one containing a fixed refresh rate and one with a modulated refresh rate (VRR flicker). The trials were controlled using the QUEST adaptive sampling method [Watson and Pelli 1983] (40 trails), implemented in PsychoPy [Peirce et al. 2019]. Responses were fitted to a psychometric function, and the contrast level at which a 0.75 correct response probability was reached was selected as the threshold contrast C_t for a specific stimulus. The sensitivity S is then computed as the reciprocal of C_t: $S = 1/C_t$. Figure 5 shows a photograph of a participant using a chin rest when observing a stimulus on the display.

Participants. We recruited a total of 16 participants, divided into three groups. The first group consisted of 4 participants who completed experiments for all 8 F_{rrs} frequencies. The second group comprised 10 participants who only participated in experiments for the low-frequency range (F_{rrs} = 0.5, 2, 4, 8 Hz), while the third group consisted of 2 participants who solely took part in experiments for the high-frequency range (F_{rrs} = 10, 11.9, 13.3, 14.9 Hz). Through the t-test examining sensitivity across various temporal frequencies, we demonstrated that there was no significant deviation between the participants of the second and third groups ($t(3) = 0.0066, p = 0.9951, sd = 0.2449$). The experiment was approved by the departmental ethics panel.

Results. The results are shown in Figure 4. For signals of any size, sensitivity to flicker varies with temporal frequency, peaking around 8 Hz. Stimuli with larger areas result in higher sensitivities. Additionally, for stimuli with small areas, sensitivity decreases

rapidly as temporal frequency exceeds 8 Hz, while such a decrease is much smaller for stimuli with larger areas. Note that due to the contrast-luminance correlation, the luminance associated with each data point varies with the reported sensitivity.

4 MODEL

To model flicker visibility, we extend Watson's TCSF [Watson and Ahumada 2011] included in the Information Display Measurements Standard (IDMS). We decided not to extend existing CSFs, such as Barten's CSF [Barten 1999] or stelaCSF [Mantiuk et al. 2022], for three primary reasons. First, CSFs introduce spatial frequency dependency, posing challenges in integrating them into display flicker modeling [Ashraf et al. 2023]. Second, most sources of flicker tend to be of low spatial frequency (Table 1). The sensitivity is mostly the function of stimulus size in the low-frequency range [Savoy and McCann 1975], and the dependence on the frequency only introduces unnecessary complexity. Furthermore, for high temporal frequencies that are relevant for flicker, sensitivity is mostly invariant to spatial frequency [Watson et al. 1986] (spatial frequency only affects sensitivity at low temporal frequencies).

The original TCSF$_{IDMS}$ only considers temporal frequency ω:

$$S_{\omega,\text{IDMS}}(\omega) = \left| \xi \left[(1 + 2i\pi\omega\tau)^{-n_1} - \zeta(1 + 2i\pi\omega\kappa\tau)^{-n_2} \right] \right|, \quad (1)$$

where $\xi = 148.7, \tau = 0.00267, \kappa = 1.834, \zeta = 0.882, n_1 = 15, n_2 = 16$, which were fitted to the de Lange Dzn [1958] data. We extend it to account for three new dimensions: luminance, eccentricity, and area. The following sections explain how each new dimension is modeled. Figure 6 summarizes the computational steps.

4.1 Luminance

In dim light, contrast sensitivity increases proportionally to the square root of retinal illuminance, in accordance with the DeVries-Rose law. Conversely, in bright light, sensitivity follows Weber's law, remaining independent of illuminance [Rovamo et al. 1995]. To incorporate those findings, we adopt the castleCSF [Ashraf et al. 2024] equation for the transient channel to model luminance sensitivity:

$$S_{\mathcal{L}}(L) = k_{1,\mathcal{L}} \left(1 + \frac{k_{2,\mathcal{L}}}{L} \right)^{-k_{3,\mathcal{L}}}, \quad (2)$$

where $k_{1...3,\mathcal{L}}$ are model parameters, which will be fitted.

The increase in luminance not only increases sensitivity but also shifts the peak of the TCSF towards higher temporal frequencies. Although not explicitly modeled, this phenomenon has been confirmed in the fitting results of [Ashraf et al. 2024] (Fig. 8 in castleCSF paper, (b,ii)). It suggests that human sensitivity to high temporal frequencies increases with higher luminance. This effect is modeled as a modification to the original TCSF$_{IDMS}$ function:

$$S_\omega(\omega, L) = S_{\omega,\text{IDMS}} \left(\frac{\omega}{b_{1,\omega} + k_{1,\omega}\log_{10}L} \right), \quad (3)$$

where $k_{1,\omega}$ and $b_{1,\omega}$ are the model parameter to be fitted.

4.2 Eccentricity

As mentioned in the Introduction, the change of sensitivity with eccentricity in the flicker detection task has been debated for over 120 years. Despite numerous attempts to explain this phenomenon,

Table 1. All flicker detection datasets utilized in our experiments.

Dataset	Temporal Frequency Hz	Spatial Frequency cpd	Eccentricity deg	Luminance cd/m^2	Area deg^2	Data	Data points
Hartmann et al. [1979]	7.77 - 61.18	0	0 - 60.37	0.7 - 70	0.2 - 7.07	CFF	136
de Lange Dzn [1958]A	23.97 - 64.23	0	0	0.16-1617.8	3.14	CFF	7
Krajancich et al. [2021]	23.01 - 94.41	0.01-0.57	0 - 55.04	3 - 190	>4.71	CFF	36
Chapiro et al. [2023]	31.88 - 51.21	0	0 - 20	10 - 8000	0.79	CFF	30
de Lange Dzn [1958]B	1.51 - 66.31	0	0	0.16-1591	3.14	Sensitivity	100
Kelly [1961]	1.6 - 75	0.01	0	0.34 - 4928.7	2827.4	Sensitivity	71
Snowden et al. [1995]	0.76 - 55.72	0.1 - 1	0	0.11 - 236	8.03	Sensitivity	120
VRR Flicker (Ours)	0.5 - 14.9	0	0	0.47 - 4.13	0.2-2369.3	Sensitivity	32

such as Rovamo and Raninen [1984]'s explanation by simultaneous scaling of stimulus area (M-scaling, retinal magnification) and illuminance (F-scaling), and Hartmann et al. [1979]'s proposition that larger area and higher luminance lead to the parafovea peak, there is still no universally accepted explanation.

Recent fMRI research on the human primary visual cortex suggests that the increase of flicker sensitivity in eccentricity is associated with the transient channel, which is sensitive to higher spatial frequencies. Horiguchi et al. [2009] identified distinct spatial distributions of the sustained and transient channels. The transient channel exhibits maximal weighting in the parafovea. Himmelberg and Wade [2019] further confirmed that the peripheral visual field is more sensitive to higher frequency stimuli by analyzing the changes in a contrast semisaturation point C_{50}[3] across different time frequencies in the foveal, parafoveal, and peripheral regions of the visual cortex. Based on these findings, we can infer that the sensitivity to high temporal frequencies should increase with eccentricity. At the same time, the contrast sensitivity data suggests that the peak of the CSF decreases with eccentricity. These two trends can be reconciled only if the TCSF changes its shape with the eccentricity — it becomes flatter (slope becomes lower) as we increase the eccentricity (see Figure 16-(a)).

Eccentricity's influence on sensitivity can be divided into two aspects: the effect of eccentricity on sensitivity, which follows a simplified formulation of the pyramid of visibility [Watson 2018]:

$$S_{\text{ecc}}(e) = 10^{-k_{1,\text{ecc}}e}, \tag{4}$$

and the effect of the eccentricity on the slope S_ω:

$$S'_\omega(\omega, L, e) = S_{\omega,\text{IDMS}}\left(\frac{\frac{\omega - \omega_p}{1 + k_{2,\omega}e} + \omega_p}{b_{1,\omega} + k_{1,\omega}\log_{10}L}\right), \tag{5}$$

where $k_{1,\text{ecc}}$ and $k_{2,\omega}$ are the model parameters to be fitted, and $\omega_p = -2$ Hz is a factor to control the temporal frequency peak shift. Then, we can construct the base function elTCSF for the subsequent spatial probability summation model:

$$S_{\text{elTCSF}}(\omega, L, e) = S_{\mathcal{L}}(L)S_{\text{ecc}}(e)S'_\omega(\omega, L, e). \tag{6}$$

---

[3]C_{50} is a measure of contrast sensitivity in the visual cortex, representing the contrast level at which 50% of the full response is achieved.

4.3 Area and Spatial Probability Summation Model

Stimulus area (size) significantly impacts sensitivity, as larger stimuli activate more retinal cells. However, existing methods [Barten 1999; Mantiuk et al. 2022] often treat area as a separate parameter, assuming that eccentricity and area effects on stimuli are independent. This assumption becomes unreasonable when dealing with very large stimuli, such as a full-screen flicker in our VRR dataset, which covers a significant range of eccentricities. To account for varying eccentricity across the visual field, we use a spatial probability summation model. Specifically, we treat the visual field as a continuous function of contrast and integrate the product of contrast and sensitivity over the window $w \times h$ (in degrees):

$$E = \int_{-\frac{w}{2}}^{\frac{w}{2}} \int_{-\frac{h}{2}}^{\frac{h}{2}} (c(x,y)S(x,y))^\beta dx\,dy, \tag{7}$$

where β is the probability summation exponent (will be fitted to the data), $c(x,y)$ represents the stimulus contrast, which is independent of spatial position ($c(x,y) \equiv c$) in all datasets used. Because all datasets used have sufficiently long durations, we disregard the impact of duration. For circular stimuli (disks), we can employ polar coordinates to simplify the spatial probability summation model:

$$d(\hat{e}, r, \theta) = \sqrt{\hat{e}^2 + r^2 + 2\hat{e}r\cos(\theta)}, \tag{8}$$

$$E(\omega, L, \hat{e}, R) = c^\beta \int_0^{2\pi} \int_0^R S_{\text{elTCSF}}^\beta(\omega, L, d(\hat{e}, r, \theta))\,r\,dr\,d\theta, \tag{9}$$

where $\hat{e}$ is the distance between the disk center and the fixation point (in visual degrees), and R is the radius (in visual degrees). When the summation reaches the threshold E_{thr}, the flicker can be detected, thus the complete $S_{\text{elaTCSF}} = 1/c$ can be expressed as:

$$S_{\text{elaTCSF}}(\omega, L, \hat{e}, R) = \left(\frac{\int_0^{2\pi} \int_0^R S_{\text{elTCSF}}^\beta(\omega, L, d(\hat{e}, r, \theta))\,r\,dr\,d\theta}{E_{thr}}\right)^{\frac{1}{\beta}} \tag{10}$$

where E_{thr} is the parameter that is fitted separately per each dataset.

CFF prediction. CFF is the temporal frequency at which the sensitivity is 1. The model from Eq. (10) cannot be analytically inverted and solved for ω. Therefore, to find the CFF, we use numerical root finding in the range between 8 and 200 Hz.
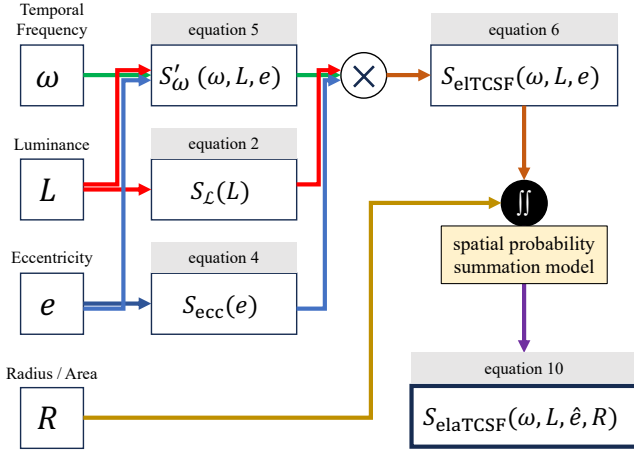
Fig. 6. The inputs (left) and computation steps of elaTCSF.

5 MODEL FITTING AND COMPARISON

In this section, we present the optimization process for all parameters of elaTCSF and compare its accuracy with the existing models.

5.1 Model Fitting

We curated numerous existing flicker detection datasets, shown in Table 1. We excluded the data points with spatial frequencies exceeding 1 cpd (as elaTCSF is meant for low spatial frequencies) and those with low luminance ($L < 0.1$ cd/m^2). In total, 8 datasets were used to train the parameters of our elaTCSF. Our optimization loss function is:

$$\mathcal{L} = \frac{1}{N} \sum_d \sum_i \left(\log_{10} S_{i,d} - s_d \log_{10} \tilde{S}_{i,d} \right)^2 + \frac{\lambda}{D} \sum_d \left(\log_{10} s_d \right)^2,$$

(11)

where $d = 1...D$ is the dataset index, i is the stimulus index in a dataset, N is the total number of stimuli, $S_{i,d}$ and $\tilde{S}_{i,d}$ are the reference and predicted sensitivity values. s_d is a per-dataset scaling factor that accounts for the difference between the datasets (differences in protocols, group of observers, etc.), as explained in stelaCSF paper[Mantiuk et al. 2022, sec. 6]. In summary, the first term of the loss function is responsible for data fitting, while the second term ensures that the per-dataset scaling factor s_d remains close to 1. In all our experiments, we fix $s_d = 1$ for our VRR dataset. We set λ to 0.001. The quasi-Newton method implemented in Matlab's *fminunc* function is used for optimization. The parameters of the fitted elaTCSF are listed in Table 2.

5.2 Model Comparison

Following the stelaCSF [Mantiuk et al. 2022] validation protocol, we perform five-fold cross-validation within each dataset, utilizing all datasets for both training and testing. We also follow the approach of other works [Ahumada et al. 2018; Watson and Ahumada 2005], reporting results for the entire dataset without a training/testing split. We report two error measures: root-mean-square-error (RMSE) of contrast sensitivity in dB units $\mathcal{E}_s$ (S-RMSE, see [Mantiuk et al. 2022, Eq. 19]) and the RMSE of CFF $\mathcal{E}_\omega$ (CFF-RMSE) in Hz. In Table 3

Table 2. The fitted parameters of elaTCSF.

Part	Parameters
TCSF$_{IDMS}$	$\xi = 154.133, \tau = 0.00292069, \kappa = 2.12547,$ $\zeta = 0.721095, n_1 = 15, n_2 = 16$
Luminance	$k_{1,\mathcal{L}} = 1.76801, k_{2,\mathcal{L}} = 1.62402, k_{3,\mathcal{L}} = 0.533781,$ $k_{1,\omega} = 0.222269, b_{1,\omega} = 0.6678$
Eccentricity	$k_{1,\text{ecc}} = 0.0330933, k_{2,\omega} = 0.0341811$
Area	$E_{thr} = 6.52801, \beta = 3.80022$

Table 3. Comparisons. S-RMSE is reported only for datasets using sensitivity as the evaluation metric, while CFF-RMSE is reported only for datasets using CFF as the evaluation metric. Regular font numbers correspond to the results of the entire dataset, while small font magenta-colored numbers represent the results of 5-fold cross-validation, indicating the mean and standard deviation across all folds. Barten's CSF (HTF) and stelaCSF (HTF) are the updated versions from [Bozorgian et al. 2024].

CSF Model	S-RMSE $\mathcal{E}_s$ [dB]	CFF-RMSE $\mathcal{E}_\omega$
TCSF$_{IDMS}$	10.33 10.38 ± 1.64	13.52 13.93 ± 1.14
Barten's CSF [Barten 1999]	5.79 6.08 ± 0.68	15.36 16.03 ± 7.77
stelaCSF [Mantiuk et al. 2022]	6.13 6.30 ± 0.36	11.47 11.82 ± 2.09
Barten's CSF (HTF)	4.58 4.82 ± 0.51	9.06 10.09 ± 1.41
stelaCSF (HTF)	6.05 6.30 ± 0.34	11.75 13.77 ± 2.25
castleCSF [Ashraf et al. 2024]	5.45 5.58 ± 0.55	13.07 14.70 ± 4.53
elaTCSF (ours)	**3.50** 3.73 ± 0.67	**8.95** 9.07 ± 1.55

we report S-RMSE results for flicker detection datasets (labelled as "Sensitivity" in Table 1) [4] and CFF-RMSE results on CFF datasets (labelled as "CFF" in Table 1).

Overall, elaTCSF outperforms the existing advanced CSF models for both error metrics. Barten's CSF (HTF) shows the best performance among the current models for the S-RMSE and CFF-RMSE. We have visualized the resulting fits in Figures 9–15.

The fitting results of elaTCSF on the de Lange Dzn [1958] (Figure 10), Kelly [1961] (Figure 11), and our VRR datasets (Figure 15) demonstrate its accuracy in predicting sensitivity values across temporal frequencies under varying luminance and stimulus size conditions. Figure 10 and Figure 11 illustrate that our elaTCSF model is applicable across a wide range of luminance levels. The results on our dataset (Figure 15), in particular, validate the effectiveness of our spatial probability summation model, as elaTCSF performs well in predicting sensitivity for both large and small stimuli.

The plots showing the fits to the datasets of Hartmann et al. [1979] (Figure 13) and Krajancich et al. [2021] (Figure 14) demonstrate that elaTCSF correctly predicts the increase of CFF in the peripheral visual field. Both datasets reveal CFF peaks within the periphery (eccentricities of 10 to 30 degrees). Although Barten's CSF (HTF) [Bozorgian et al. 2024] attempts to model these peaks, it predicts the peak eccentricities to be much lower than those observed experimentally. In contrast, our elaTCSF accurately models

---

[4]Notably, as elaTCSF does not consider spatial frequency, we used [Snowden et al. 1995] dataset exclusively as the training set and excluded it during model comparison.
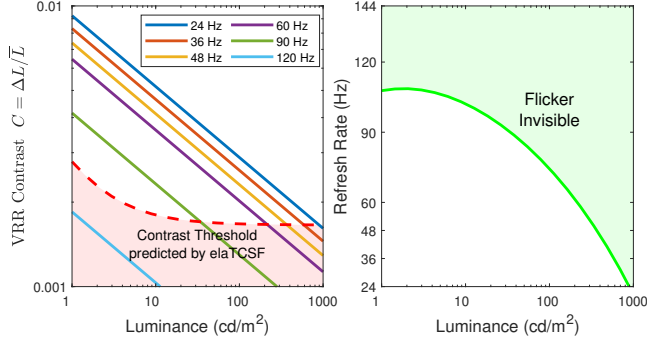
Fig. 7. Left: Measured/simulated contrast of VRR flicker when switching between 144 Hz and given refresh rate (lines). The dashed line is the detection threshold predicted by elaTCSF for the given display. Right: The pale green area is the range of refresh rates in which the display can operate without visible flicker. The lower bound of that range is the intersection of the contrast lines with the threshold, in the plot on the left. Note that higher luminance makes VRR flicker less visible because of the reduced VRR-flicker contrast.

the parafoveal CFF peaks. While there are deviations at very low luminance and high eccentricities (Figure 13), the predictions made by elaTCSF are sufficiently accurate for practical applications.

The datasets of de Lange Dzn [1958] (Figure 9) and Chapiro et al. [2023] (Figure 12) demonstrate the relationship between CFF and luminance, including very high luminance levels (up to 8000 cd/m^2), which is beneficial for HDR display design. While elaTCSF outperforms existing models, it is inconsistent with the dataset of Chapiro et al. [2023]. According to their data, the CFF values at fovea (0 degree) are higher than those in the parafoveal regions (10, 20 degrees), which is inconsistent with the trends observed in the datasets of Krajancich et al. [2021] and Hartmann et al. [1979]. The factors that could cause this inconsistency between the datasets are unknown and, consequently, cannot be modeled.

6   APPLICATIONS

The primary application elaTCSF addresses is VRR flicker, which we measured and then validated our model on. Below in Section 6.1 we demonstrate how VRR flicker can be mitigated in practice. We also show how elaTSCF can be used to predict flicker in VR/AR headsets (Section 6.2), and how it can serve as a better flicker model for lighting design (Section 6.3). The latter two application, however, are not valiated.

6.1   Prediction of Frame Rate Range for VRR Displays

A common method to mitigate VRR flicker is to limit the operational range of frame rates when VRR is enabled. For instance, even if the monitor supports the range from 24 Hz to 144 Hz, it is restricted to 40 Hz to 144 Hz in the VRR mode using low frame rate compensation (LFC). This approach reduces flicker visibility by minimizing potential luminance differences between frame rates. Currently, without a robust model, engineers manually adjust the refresh rate range until the flicker cannot be noticed.

Our elaTCSF can calculate the flicker-free refresh rate range for VRR displays at different luminance levels. In this example, we will
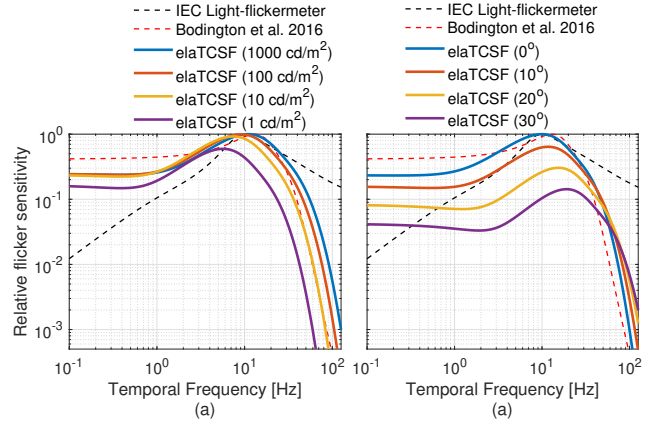

Fig. 8. Comparison of relative flicker sensitivity functions from the IEC Light-flickermeter and [Bodington et al. 2016] with the predictions of elaTCSF model at (a) various luminance levels for a foveal visual field of 1000 degrees^2, and (b) fovea and different peripheral eccentricities for visual fields of 100 degrees^2 and 1000 cd/m^2. The model predictions are normalised with respect to the maximum sensitivity from 1000 cd/m^2 condition for plot (a), and the foveal condition for plot (b).

simulate a 27-inch 24–144 Hz display. First, following our procedure from Section 3, we need to measure for each luminance level the contrast introduced by switching from the 144 Hz (maximum) to any other frame rate. Such contrast for our simulated display is shown as lines in Figure 7. Then, we use elaTCSF to find the detection threshold for the display across the luminance range, shown as a dashed line in Figure 7-left. We use the maximum sensitivity across all temporal frequencies to ensure conservative thresholds. The intersection of the VRR-flicker contrast lines with the threshold gives us the lower bound of the refresh rate, shown as the green line in Figure 7-right. The pale green area indicates the range of refresh rates in which VRR can operate without introducing visible flicker.

6.2   Low persistence flicker in VR headsets

VR headsets display world-locked content that can move rapidly with head motion. Because of that, they are prone to hold-type blur [Rao et al. 2024]. Such blur can be much reduced using a low-persistence display, which keeps the image on for a fraction of the frame duration (e.g., 2 ms for a 7 ms frame) and the display remains black for the remaining time. This introduces the stroboscopic effect, making the image appear sharper, but it can introduce visible and uncomfortable high-contrast flicker. Currently, VR manufacturers rely solely on empirical evidence to set the lower limit for refresh rates, such as Meta's assertion [Rao et al. 2024] that 90 Hz is the minimum refresh rate for a comfortable user experience.

As our elaTCSF accounts for all relevant factors, we can predict the minimum refresh rate of a VR headset that ensures the low-persistence flicker remains invisible. Based on publicly available data regarding device's FoV, we predicted CFF for three headsets: Apple Vision Pro, Microsoft HoloLens 2 and Meta Quest 3. We plot CFF as the function of luminance in the Figure 1-right. The predicted values assume that the display is showing a uniform field of a given luminance. If the display's refresh rate is above the CFF line, the

low-persistence flicker is unlikely to be visible. The plots show how much the refresh rate would need to increase if we wanted to increase the display peak luminance without introducing flicker.

6.3 Application in lighting design

Flicker in lighting systems has long been a concern, initially identified with old incandescent bulbs. While advances in lighting technology, particularly with LEDs, have mitigated some flicker issues, they have not been completely resolved. Modern LED lights use a range of driver circuits to manage voltage fluctuations and flicker can still be present due to the type of LED driver used and its handling of voltage fluctuations [Collin et al. 2019]. Changes in voltage supply can still produce perceptible flicker, especially with less efficient driver circuits. LED products can also exhibit flicker at dim light levels or during transitions between dimming states [Poplawski and Miller 2013]. The current standards for estimating the flicker index of light sources, such as those set by the International Electrotechnical Commission (IEC), rely on human contrast sensitivity measurements developed for incandescent lighting. These standards do not fully account for the differences in flicker sensitivity under varying lighting conditions [IEC 2010, 2020]. Our elaTCSF model, supported by recent measurements can be used to update the current standards. A recent work by [Kukačka et al. 2023] highlighted the importance of incorporating human TCSF measurements in the light flicker index (LFI) for different light sources.

Figure 8 shows the prediction of our model versus the filter used in the IEC standard and from another TCSF measurement [Bodington et al. 2016]. The filter used in IEC standard is from [Drápela and Šlezingr 2010] and the measurements from [Bodington et al. 2016] have been used in a recommendation to update the current lighting standards [ASSIST 2015]. Both TCSF measurements from the literature do not show any variation with luminance, eccentricity, etc., whereas our model is able to predict changes in flicker sensitivity with different viewing conditions. This capability can be used to update lighting flicker index measurements for different conditions, providing a more comprehensive and perceptually-accurate framework for assessing flicker in modern lighting systems.

7 CONCLUSIONS

A flickering light source, such as a display or lighting, can be very annoying, cause eye strain and headaches, and is a main concern in display and lighting design. A certain amount of flicker is unavoidable. Therefore, the main question is what is the largest contrast or the smallest temporal frequency at which the flicker becomes invisible. To that end, we proposed elaTCSF, which can predict both. It accounts for all main factors that influence flicker perception: temporal frequency, luminance, eccentricity and size. This is a significant improvement over existing models, which cannot predict the threshold contrast (e.g., CFFs), do not account for all relevant factors (e.g., IDMS TCSF), or do not offer sufficient accuracy (e.g., stelaCSF). elaTCSF is fitted to and tested against 8 different datasets with both CFF and sensitivity measurements, one of which we collected specifically to address the prominent issue of flicker in VRR displays. elaTCSF is built on established psychophysical models, such as Watson's TCSF, or the spatial probability summation. This

choice was made to avoid overfitting given the sparsity of available psychophysical data. Even if a better fit can be found with a polynomial function or a neural network, such a function is unlikely to generalize to the conditions outside the training dataset.

The main limitation of elaTCSF is that it can only predict flicker for low-spatial-frequency or large patterns, as it does not account for spatial frequency. We found that this compromise was necessary to achieve both good quantitative and qualitative predictions, and because the previous attempts to extend more complex CSFs were not fully successful [Bozorgian et al. 2024]. elaTCSF is trained and validated on VRR flicker data as this is the focus of our work. The model is yet to be validated on other applications, including flicker of low-persistence displays and flicker in lighting design.

REFERENCES

Albert Ahumada, Jihyun Yeonan-Kim, and Andrew B Watson. 2018. A Dual Channel Spatial-Temporal Detection Model. *Electronic Imaging* 30 (2018), 1–4.

Maliha Ashraf, Rafal Mantiuk, and Alexandre Chapiro. 2023. Modelling contrast sensitivity of discs. *Electronic Imaging* 35 (2023), 1–8.

Maliha Ashraf, Rafał K Mantiuk, Alexandre Chapiro, and Sophie Wuerger. 2024. castleCSF—A contrast sensitivity function of color, area, spatiotemporal frequency, luminance and eccentricity. *Journal of Vision* 24, 4 (2024), 5–5.

ASSIST. 2015. Recommended metric for assessing the direct perception of light source flicker. *ASSIST Recommends* (2015), 1–18.

Peter GJ Barten. 1999. *Contrast sensitivity of the human eye and its effects on image quality.* SPIE press.

D Bauer, M Bonacker, and CR Cavonius. 1983. Frame repetition rate for flicker-free viewing of bright VDU screens. *Displays* 4, 1 (1983), 31–33.

D Bodington, A Bierman, and N Narendran. 2016. A flicker perception metric. *Lighting Research & Technology* 48, 5 (2016), 624–641.

Ali Bozorgian, Maliha Ashraf, and Rafal Mantiuk. 2024. Spatiotemporal contrast sensitivity functions: predictions for the critical flicker frequency. *Electronic Imaging* 36 (2024), 1–8.

Bruno Breitmeyer and Bela Julesz. 1975. The role of on and off transients in determining the psychophysical spatial frequency response. *Vision Research* 15, 3 (3 1975), 411–415. https://doi.org/10.1016/0042-6989(75)90090-5

Alexandre Chapiro, Nathan Matsuda, Maliha Ashraf, and Rafal Mantiuk. 2023. Critical Flicker Frequency (CFF) at high luminance levels. *Electronic Imaging* 35 (2023), 1–5.

Adam J Collin, Sasa Z Djokic, Jiri Drapela, Roberto Langella, and Alfredo Testa. 2019. Light flicker and power factor labels for comparing LED lamp performance. *IEEE Transactions on Industry Applications* 55, 6 (2019), 7062–7070.

PM Daniel and D Whitteridge. 1961. The representation of the visual field on the cerebral cortex in monkeys. *The Journal of physiology* 159, 2 (1961), 203.

H de Lange Dzn. 1958. Research into the dynamic nature of the human fovea→ cortex systems with intermittent and modulated light. I. Attenuation characteristics with white and colored light. *Josa* 48, 11 (1958), 777–784.

Kristian Donner. 2021. Temporal vision: Measures, mechanisms and meaning. https://doi.org/10.1242/jeb.222679

Jiří Drápela and Jan Šlezingr. 2010. A light-flickermeter–part I: design. In *Proceedings of the 11th International Scientific Conference Electric Power Engineering 2010.* 453–458.

Arthur A Eastman and John H Campbell. 1952. Stroboscopic and flicker effects from fluorescent lamps. *Illuminating Engineering* 47, 1 (1952), 27–35.

Joyce E. Farrell. 1986. An analytical method for predicting perceived flicker. *Behaviour and Information Technology* 5, 4 (1986), 349–358. https://doi.org/10.1080/01449298608914528

Ragnar Granit and Phyllis Harper. 1930. Comparative studies on the peripheral and central retina: II. Synaptic reactions in the eye. *American Journal of Physiology-Legacy Content* 95, 1 (1930), 211–228.

E Hartmann, B Lachenmayr, and H Brettel. 1979. The peripheral critical flicker frequency. *Vision Research* 19, 9 (1979), 1019–1023.

Selig Hecht and Cornelis D Verrijp. 1933. Intermittent stimulation by light: III. The relation between intensity and critical fusion frequency for different retinal locations. *The Journal of general physiology* 17, 2 (1933), 251–268.

Marc M Himmelberg and Alex R Wade. 2019. Eccentricity-dependent temporal contrast tuning in human visual cortex measured with fMRI. *NeuroImage* 184 (2019), 462–474.

Hiroshi Horiguchi, Satoshi Nakadomari, Masaya Misaki, and Brian A Wandell. 2009. Two temporal channels in human V1 identified using fMRI. *Neuroimage* 47, 1 (2009), 273–280.

BS Hylkema. 1942. Examination of the visual field by determining the fusion frequency. *Acta Ophthalmologica* 20, 2 (1942), 181–193.

IEC. 2010. IEC 61000-4-15:2010 Electromagnetic compatibility (EMC) Part 4–15: Testing and Measurement Techniques—Flickermeter—Functional and Design Specifications. *IEC (International Electrotechnical Commission) Standard 61000* (2010), 1–58.

IEC. 2020. *IEC TR 61547-1:2015 Equipment for General Lighting Purposes–EMC Immunity Requirements–Part 1: An Objective Light Flickermeter and Voltage Fluctuation Immunity Test Method.* Technical Report. IEC (International Electrotechnical Commission) TR 61547-1. Geneva: IEC.

DH Kelly. 1961. Visual responses to time-dependent stimuli.* I. Amplitude sensitivity measurements. *JOSA* 51, 4 (1961), 422–429.

Xiangzhen Kong, Mijael R Bueno Perez, Ingrid MLC Vogels, Dragan Sekulovski, and Ingrid Heynderickx. 2018. Modelling contrast sensitivity for chromatic temporal modulations. In *Color and Imaging Conference*, Vol. 26. Society for Imaging Science and Technology, 324–329.

Brooke Krajancich, Petr Kellnhofer, and Gordon Wetzstein. 2021. A perceptual model for eccentricity-dependent spatio-temporal flicker fusion and its applications to foveated graphics. *ACM Transactions on Graphics (TOG)* 40, 4 (2021), 1–11.

Leoš Kukačka, Jan Hergesel, Jakub Nečásek Petr Bílek, Michal Vik, Jan Meyer, Robert Stiegler, and Jiří Drápela. 2023. Comparison of Procedures for Measuring the Temporal Contrast Sensitivity Function. In *2023 IEEE Sustainable Smart Lighting World Conference & Expo (LS18)*. IEEE, 1–6.

Brad Lehman, Arnold Wilkins, Sam Berman, Michael Poplawski, and Naomi Johnson Miller. 2011. Proposing measures of flicker in the low frequencies for lighting applications. In *2011 IEEE Energy Conversion Congress and Exposition*. IEEE, 2865–2872.

Rafał K Mantiuk, Maliha Ashraf, and Alexandre Chapiro. 2022. stelaCSF: a unified model of contrast sensitivity as the function of spatio-temporal frequency, eccentricity, luminance and area. *ACM Transactions on Graphics (TOG)* 41, 4 (2022), 1–16.

Naomi J Miller, Felipe A Leon, Jianchuan Tan, and L Irvin. 2023. Flicker: A review of temporal light modulation stimulus, responses, and measures. *Lighting Research & Technology* 55, 1 (2023), 5–35.

Jonathan Peirce, Jeremy R Gray, Sol Simpson, Michael MacAskill, Richard Höchenberger, Hiroyuki Sogo, Erik Kastman, and Jonas Kristoffer Lindeløv. 2019. PsychoPy2: Experiments in behavior made easy. *Behavior research methods* 51 (2019), 195–203.

Gilbert Phillips. 1933. Perception of flicker in lesions of the visual pathways. *Brain* 56, 4 (1933), 464–478.

ME Poplawski and NM Miller. 2013. Flicker in solid-state lighting: Measurement techniques, and proposed reporting and application criteria. In *Proceedings of CIE Centenary Conference "Towards a new century of light". Paris, France.* sn, 4.

Thomas Conrad Porter. 1902. Contributions to the study of flicker. Paper II. *Proceedings of the Royal Society of London* 70, 459-466 (1902), 313–329.

Linghui Rao, Naamah Argaman, Jim Zhuang, Ajit Ninan, Cheonhong Kim, Daozhi Wang, and Shizhe Shen. 2024. Display and Optics Architecture for Meta's AR/VR Development. *IEEE Open Journal on Immersive Displays* (2024).

Andrew T. Rider, G. Bruce Henning, and Andrew Stockman. 2019. Light adaptation controls visual sensitivity by adjusting the speed and gain of the response to light. *PLoS ONE* 14, 8 (8 2019), e0220358. https://doi.org/10.1371/journal.pone.0220358

J. G. Robson. 1966. Spatial and Temporal Contrast-Sensitivity Functions of the Visual System. *Journal of the Optical Society of America* 56, 8 (8 1966), 1141. https://doi.org/10.1364/josa.56.001141

Robert T Ross. 1936. The fusion frequency in different areas of the visual field: II. The regional gradient of fusion frequency. *The Journal of General Psychology* 15, 1 (1936), 161–170.

Jyrki Rovamo, Juvi Mustonen, and Risto Näsänen. 1995. Neural modulation transfer function of the human visual system at various eccentricities. *Vision Research* 35, 6 (1995), 767–774.

Jyrki Rovamo and Antti Raninen. 1984. Critical flicker frequency and M-scaling of stimulus size and retinal illuminance. *Vision research* 24, 10 (1984), 1127–1131.

Michele Rucci, Ehud Ahissar, and David Burr. 2018. Temporal Coding of Visual Space. *Trends in Cognitive Sciences* 22, 10 (10 2018), 883–895. https://doi.org/10.1016/J.TICS.2018.07.009

Robert L. Savoy and John J. McCann. 1975. Visibility of low-spatial-frequency sine-wave targets: Dependence on number of cycles. *Journal of the Optical Society of America* 65, 3 (March 1975), 343. https://doi.org/10.1364/JOSA.65.000343

Gerrit A Slavenburg, Marcel Janssens, Luis Lucas, Robert Jan Schutten, and Tom Verbeure. 2020. 46-1: Invited Paper: Variable Refresh Rate Displays. In *SID Symposium Digest of Technical Papers*, Vol. 51. Wiley Online Library, 669–672.

Robert J. Snowden, Robert F. Hess, and Sarah J. Waugh. 1995. The processing of temporal modulation at different levels of retinal illuminance. *Vision Research* 35, 6 (3 1995), 775–789. https://doi.org/10.1016/0042-6989(94)00158-I

Christopher W Tyler. 1987. Analysis of visual modulation sensitivity. III. Meridional variations in peripheral flicker sensitivity. *JOSA A* 4, 8 (1987), 1612–1619.

Andrew B Watson. 2018. The field of view, the field of resolution, and the field of contrast sensitivity. *Electronic Imaging* 30 (2018), 1–11.

Andrew B Watson et al. 1986. Temporal sensitivity. *Handbook of perception and human performance* 1, 6 (1986), 1–43.

Andrew B Watson and Albert J Ahumada. 2005. A standard model for foveal detection of spatial contrast. *Journal of vision* 5, 9 (2005), 6–6.

Andrew B Watson and Albert J Ahumada. 2011. flicker visibility: a perceptual metric for display flicker. In *SID symposium digest of Technical Papers*, Vol. 42. Wiley Online Library, 957–959.

Andrew B Watson and Albert J Ahumada. 2015. 5.3: Extending the Flicker Visibility Metric to a Range of Mean Luminance. In *SID Symposium Digest of Technical Papers*, Vol. 46. Wiley Online Library, 30–32.

Andrew B Watson and Denis G Pelli. 1983. QUEST: A Bayesian adaptive psychometric method. *Perception & psychophysics* 33, 2 (1983), 113–120.

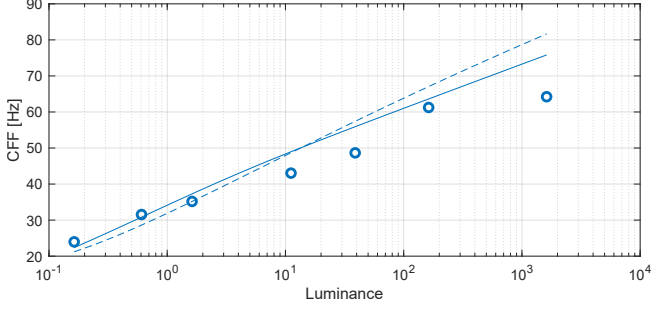Fig. 9. Predictions for [de Lange Dzn 1958] dataset (CFF). Continuous lines: elaTCSF; dashed lines: Barten's CSF (HTF).
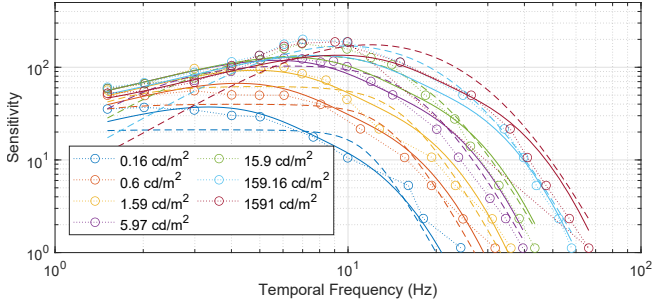

Fig. 13. Predictions for [Hartmann et al. 1979] dataset. Continuous lines: elaTCSF; dashed lines: Barten's CSF (HTF).

Fig. 10. Predictions for [de Lange Dzn 1958] dataset (Sensitivity). Continuous lines: elaTCSF; dashed lines: Barten's CSF (HTF).
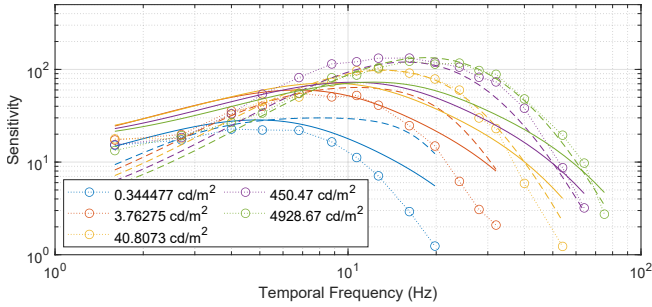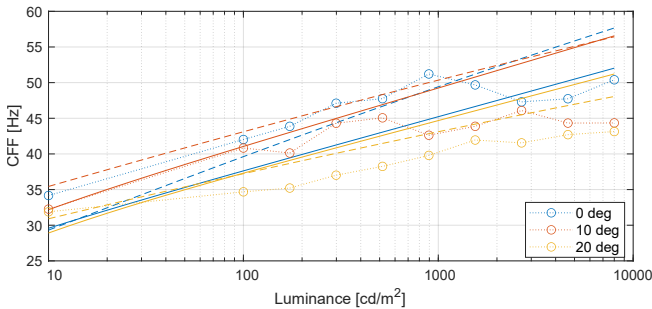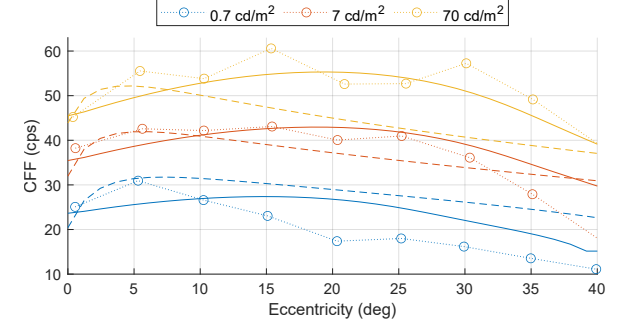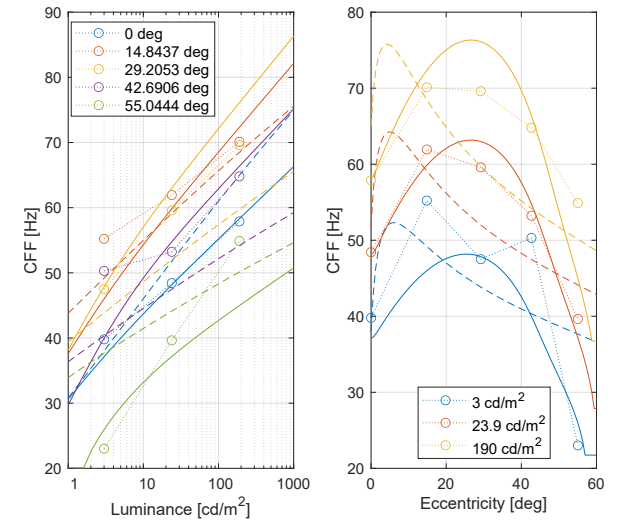

Fig. 14. Predictions for [Krajancich et al. 2021] dataset. Continuous lines: elaTCSF; dashed lines: Barten's CSF (HTF).

Fig. 11. Predictions for [Kelly 1961] dataset. Continuous lines: elaTCSF; dashed lines: Barten's CSF (HTF).

Fig. 12. Predictions for [Chapiro et al. 2023] dataset. Continuous lines: elaTCSF; dashed lines: Barten's CSF (HTF).
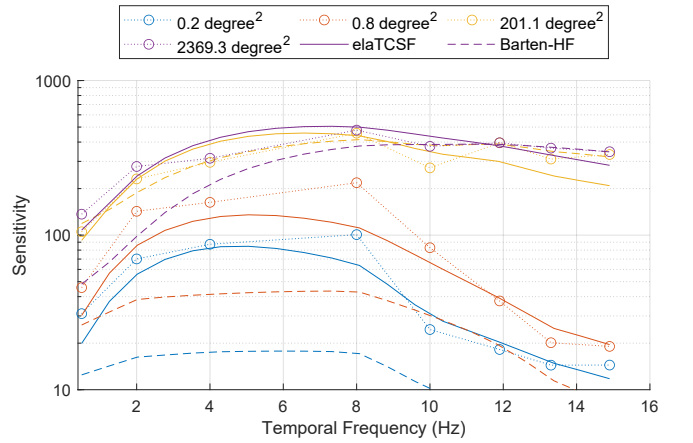

Fig. 15. Predictions for our VRR dataset (Temporal Frequency). Continuous lines: elaTCSF; dashed lines: Barten's CSF (HTF) [Bozorgian et al. 2024].
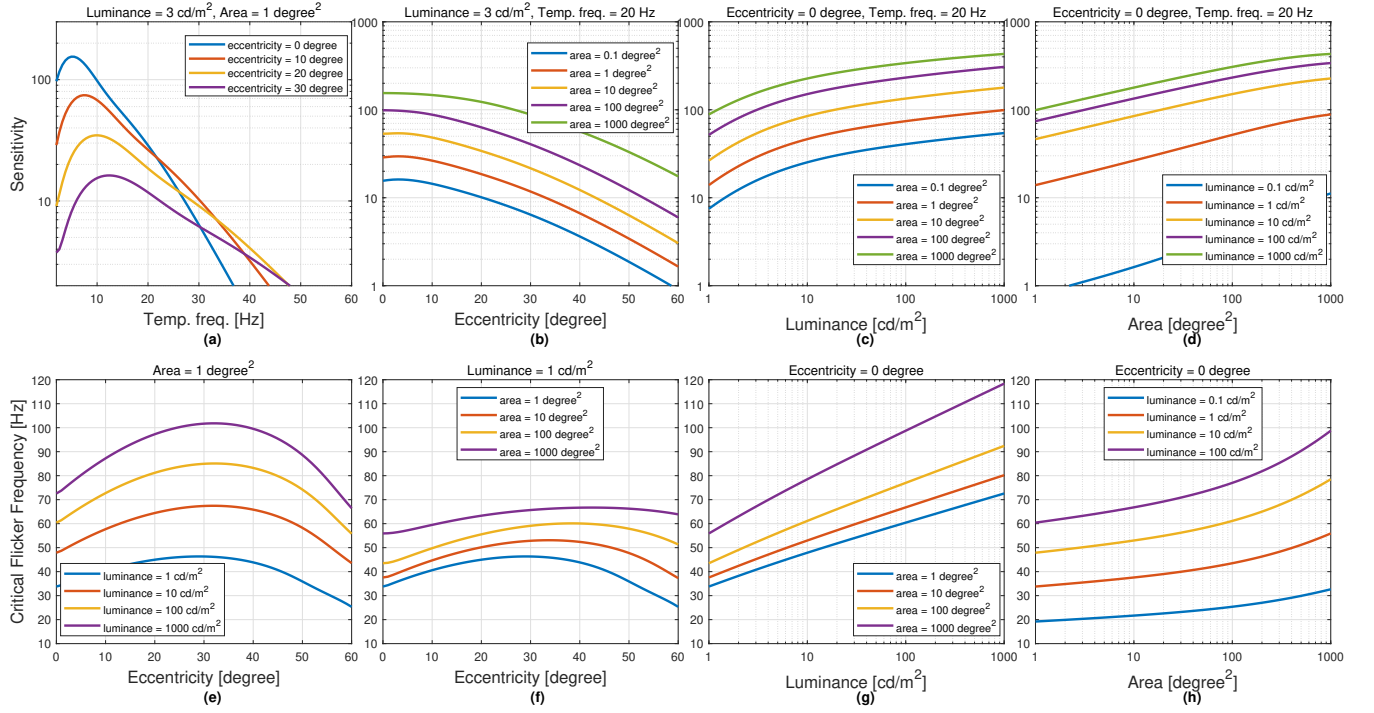
Fig. 16. The sensitivity (first row) and critical flicker frequency (second row) computed for elaTCSF under different conditions.